HIGH STRAIN RATE RESPONSE AND DEFORMATION MECHANISMS IN KINKING NONLINEAR ELASTIC SOLIDS: MAX PHASE TERNARY CERAMICS

R. Bhattacharya[1] and N. C. Goulbourne[2*]

[1]*Materials Science and Engineering, University of Michigan, Ann Arbor, MI*
[2] *Aersospace Engineering, University of Michigan, Ann Arbor, MI*
**ngbourne@umich.edu*

Keywords: Split Hopkinson Pressure Bar, high strain rate, ternary ceramics.

Abstract

The present study is concerned with understanding the high strain rate deformation mechanisms and the role of microstructural characteristics in $M_{n+1}AX_n$ phase ternary ceramics. These materials crystallize in a Hexagonal Close Packed (HCP) structure with a c/a ratio greater than 1.67 which results in kink band formations when subjected to loading. In this work, we report the high strain rate deformation and fracture mechanisms observed in Ti_2AlC, a ternary ceramic, when subjected to dynamic compressive loading (~1200 s^{-1}) using a Split Hopkinson Pressure Bar (SHPB) technique and 2-D high speed Digital Image Correlation (DIC) to measure in-plane displacements. Specimens with different geometries are tested due to the tendency of these materials to fracture prematurely and also due to lack of established experimental protocols for testing ternary ceramics using SHPB (in comparison to metals, ceramics, polymers), which is another objective of the study. The fractography analysis, done using a Scanning Electron Microscope (SEM), reveals the dominant fracture mechanisms to consist of kink band formations, grain folding and delamination, cavity formation, delamination of the nano-laminates, grain pullout, and tearing etc. These features, though observed under static loading conditions, initiate and propagate in the material by a completely different mechanism. Qualitative and quantitative comparison show dynamic loading leads to more *advanced* deformation modes.

1 Introduction

$M_{n+1}AX_n$ phase materials represent layered ternary ceramics where M is an early transition metal, A is an A-group element and X is C or N. The value of n typically varies from 1 to 3 [1-3]. These materials, like many carbides, show high temperature stability of up to 2000^{o}C [1, 3] but with increased machinability and ductility. This unique combination of properties makes them attractive materials for structural applications at room and elevated temperatures. These materials are also classified as Kinking Nonlinear Elastic (KNE) solids, which have a hexagonal crystal structure [4]. Such behavior can be attributed to the hexagonal structure with a high c/a ratio, greater than 1.67, and hence these materials deform by extensive kink band formations [2-6]. Ti_2AlC is one such material which belongs to this class of layered ternary KNEs. While the behavior and response of these materials under quasi-static loading conditions (10^{-4} s^{-1}) has been investigated [3,7,8], mechanical dynamic characterization has

not been reported. In this paper we report on the high strain rate (up to ~ 2000 s^{-1}) response using a Split Hopkinson Pressure Bar (SHPB) technique.

SHPB testing is typically used to characterize the constitutive stress-strain response in a material at high strain rates (10^2 - 10^4 s^{-1}) [9]. The data reduction technique is based on assumptions that deformation in the specimen is: i) uniform and evenly distributed, ii) the mechanical impedance of the material tested is similar to the incident/transmission bar, iii) the bars remain elastic, a uniaxial stress state exists in the specimen and the material is isotropic, homogenous, and without inherent flaws. Since the test is material dependent, proper specimen design is important [10], especially for hard and brittle ceramics. Any flaw in these materials would lead to premature failure and hence lead to an erroneous measurement of the stress-strain response. Therefore, a tolerance to high degree of flatness and parallelism of the specimens is recommended. The typical values of length-diameter ratio have been recommended to be between 0.5 and 1 for metals, and between 1 and 2 for ceramics [11]. The specimens can be tested under different loading modes such as compression, tension, torsion at both room temperature as well as elevated temperatures [12]. All the tests reported in this paper are conducted under compressive loading. Further details regarding this technique, specimen preparation and experimental set-up are presented in a subsequent section. Apart from measuring and calculating the strains using strain-gauge signals, a full field method, 2D Digital Image Correlation (DIC) was used (the high speed camera capability is up to a frame rate of 1 million frames per second).

The principle of DIC is based on the identification of an object point on the surface of the material being tested using an indistinguishable intensity pattern, which is applied to the material before testing (speckle patterning). A correlation step then divides the images into several sub-images known as facets. At every loading step, the facet deformation is tracked. In 2D DIC, only one camera is used whereas 3D DIC involves two cameras, in which the correlation algorithm first performs the task of finding a homologous point on the surface of the specimen, from images obtained from the two cameras [19-24]. In this paper we report 2D DIC at high speeds (10^5 frames per second) and hence neglect any out-of-plane motions. The specimen is therefore assumed to be nominally planar and deforms only in the original object plane. Though this method is highly advanced and uses a non-contact algorithm to calculate the strain fields, errors due to image distortion and correlation are possible. Distortion is the deviations in the image position with respect to a specific model. The sources of distortion could be from the aberrations of the lenses and misalignment of optical elements. Parametric models have been developed to correct these distortions and these methods are dealt with and described in detail in [22]. Correlation errors are typically classified into statistical and systematic errors. Statistical errors are due to camera image noise and also due to a limited number of pixels caused by camera digitization. Systematic errors are correlation errors caused by several reasons when the facet transformation model does not consider the real situation. This error creeps into measurements when a curved specimen surface is analyzed using DIC, assuming planar surface. This situation is particularly relevant to the tests reported here since cylindrical specimens, having a curved cross-section are analyzed using 2D DIC. A more detailed discussion of this error and ways to tackle them is presented elsewhere [23] and not considered here further.

This paper is organized into 3 broad sections, with sub-sections. Section 2 outlines the experimental steps with sub-section 2.1 describing the sample preparation, with sub-sections 2.2 and 2.3 outlining a detailed description of the SHPB set up used for the tests, coupled with the high speed camera, data processing and analysis, etc. The results and discussions from the

tests are reported in Section 3, with sub section 3.1 reporting the strain calculations and the constitutive stress-strain behavior of Ti_2AlC under high strain rate loading. The microstructural analysis of the specimens before and after deformation (with and without fracture) is reported in 3.2 and a discussion on the results is presented in 3.3. Section 4 outlines the conclusions from the results obtained with possible scope and direction of future work.

2 Materials and testing methods

2.1 Sample Preparation

The material used in this work is polycrystalline Ti_2AlC, which was received from Texas A&M University (TAMU-MURI 18 team lead and collaborator). The material has been synthesized using a pressureless sintering process. The details of the synthesis process can be found in [1-7, 26]. Cylindrical specimens were received with a diameter of 12.7 mm (0.5 inches), which was prepared for SHPB testing, using Electro Discharge Machining (EDM) to ensure perfectly flat and smooth surfaces with minimal flaws. Specimens with Length (L)-Diameter (D) ratios of 0.2, 0.4 and 0.8 were tested to study the effect of specimen size on the high strain rate response of the material. The ratios were decided based on reported literature [16-20] on SHPB testing in ceramics and ductile metals, since MAX phase materials exhibit a unique combination of both properties. The microstructure of the specimens before and after deformation and fracture was examined and the results are presented in a subsequent section. The specimens were speckled with black paint on a white coating to provide the contrast for subsequent analysis using DIC.

2.2 SHPB EXPERIMENTAL SET-UP

The Split Hopkinson Pressure Bar (SHPB) set up consists of two bars, an incident bar and a transmission bar, on which strain gauges are placed. The specimen is “sandwiched” between the two bars. The strain pulses obtained from the test are analyzed and processed assuming 1D wave propagation theory[12, 13]. A 2-wave analysis was been used to process the strain pulses and obtain dynamic stress-strain curves. The strain in the material was calculated both using strain gages on the bars as well as using a high speed DIC method. This method of analyzing the data to calculate the strain is free from the errors due to assumptions included in the wave analysis of the strain pulse signals. However for the sake of simplicity, 2D DIC was used in this study, which can measure only in-plane displacements thus neglecting out-of-plane motion. Since a cylindrical specimen with curve surface is used, this method is not fully accurate and can be improved by a) using 2 cameras and 3D DIC, b) 3D DIC using one camera [22] or c) using a specimen with planar (rectangle/square) cross section [15].

3. Results and Discussion

3.1 Strain Fields

Cylindrical specimens of three different L-D ratios were machined from a bulk cylindrical specimen. Tests were conducted using the two different experimental set-ups on these specimens to determine the effect of specimen geometry on the response of these materials. A comparison between the strains calculated using DIC and that calculated from analysis of gauge data shows some mismatch (error ~ 5%). The trend, however, is similar i.e. the strain gauge signals overlap well with the DIC calculations during the rise time but shows some deviation and goes to relatively higher strains.

Figure 1 shows the stress-strain behavior of tests done at L-D ratios of 0.2 and 0.4. The stress-strain behavior at an L-D ratio 0.8 cannot be used to calculate the modulus of the material due to the premature propagation of cracks and subsequent fracture, which will be treated separately in a subsequent section. The stress-strain curves reveal that the material goes to

higher strain value at lower L-D ratios. It also clearly shows that specimens having identical L-D ratios, when tested at different strain rates, reach higher stress values at higher strain rates. The stress-strain plots shown in Figure 1 also shows a strain rate dependence of the behavior. There is some amount of ductility in the specimens due to which it yields and deforms plastically. No definite yield point was observed in the specimen with L-D ratio 0.4 tested at 500 s^{-1}. For a given L-D ratio, it is observed that the yield strength increases with increasing strain rate. Yielding occurs in these materials due to formation of fully formed kink bands which are permanent microstructural rearrangements and cause plastic deformation behavior. The curve termination points do not depict fracture of the material but a loss of contact of the specimen with the bars. The maximum elongation in the material does not have a systematic variation with strain rate. However it is observed that thicker specimens elongate less compared to a specimen with lower L-D ratio. The behavior reveals strain hardening, with the rate of hardening being higher compared to that of a metal.

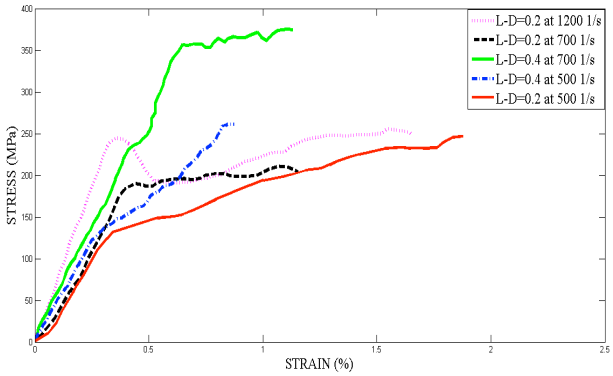

Figure 1. Stress-Strain behavior at high strain rates showing effect of varying Length (L)-Diameter (D) ratio and strain rate.

Figure 2 shows the strain fields in the x direction for a specimen tested at L-D ratio of 0.4, at different time intervals of 10 µs. The scale (shown on the last image of each row) is uniform for all the images in the series and has a range of 0mm to 0.1mm (in the negative sense indicating compression in the x direction) for the displacement. The strain field heterogeneity between the "hot spots" and "cold spots" are within a range of 0.3-0.4%. Based on microstructural characterization of the deformed specimens (without obvious macroscale fracture), which show numerous rough area formations throughout the surface, we hypothesize that these rough areas act as sources of stress concentrations and are "hot-spots".

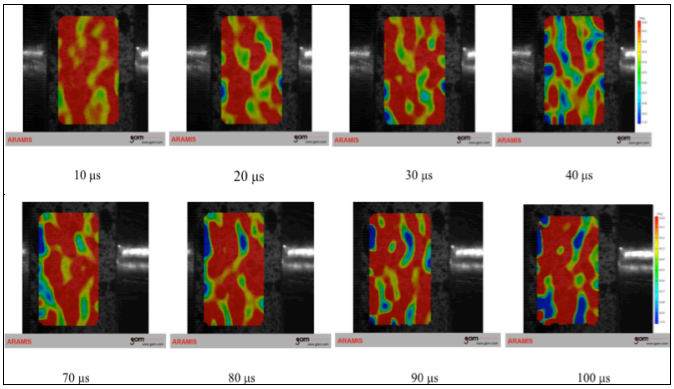

Figure 2. Strain field in x direction for specimen of L-D ratio 0.4, at time intervals of 10µs, starting with 10 µs from the start of the test. Scale: 0 (Red) to 1 (Blue) % (Negative x direction).

Figures 3 shows the strain fields for the same specimen in the perpendicular direction. The displacement, as is expected, is tensile in the y direction, with values smaller than the displacement in the x direction. Heterogeneities in the range 0.3-0.4% are observed throughout the surface of the specimen.

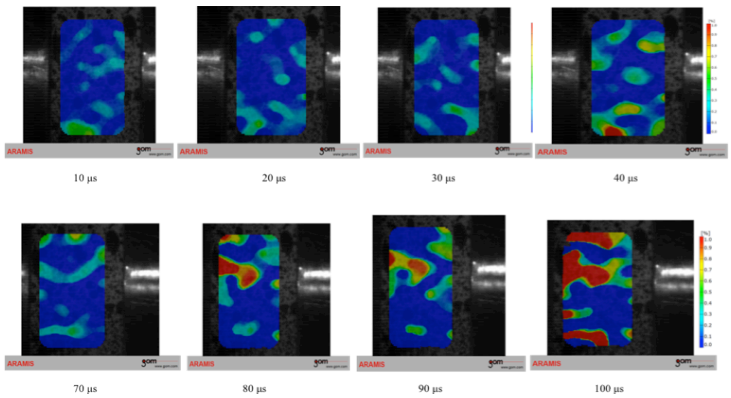

Fig 3. Strain fields in the y direction for a specimen of L-D ratio 0.4, at time intervals of 10µs, starting with 10 µs from the start of the test, shows heterogeneity in the strains. Scale: 0 (Blue) to 1 (Red) % (Positive y direction)

3.2 Dynamic Deformation Mechanisms

In this section, microscopic characterization of the material before and after deformation is presented to reveal the microstructural features and provide necessary information to relate the microstuctural mechanisms to the deformation observed at macroscale. The microstructure before deformation, shown in Fig 4 are obtained by etching it in a solution containing HCl, HNO_3 and H_2O in the proportion 1:1:1, which revealed the grain and layered structure in the material. Inclusions in the form of TiC particles and small dark spots were seen distributed in the optical micrographs (shown in black). The nanoscale spots (~1 nm) could have been possibly formed during processing of the specimens. The inclusions were distinguished from pits using SEM. An SEM micrograph, shown in Fig 4, distinguishes the TiC particles as bright zones from the dark pits, shown as black spots. The grains and layered regions have a random orientation and a distribution of sizes. The deformed morphology of the specimens (L-D=0.4) shown in Fig 5 revealed numerous rough patches (much larger than pits observed in Fig 4) throughout the surface of the specimen, which are possible areas of stress concentration. These patches are areas on the surface of the specimen from where surface smoothness achieved after machining was lost.

3.2.1 Microstructural Characterization

This sub-section demonstrates the surface condition (etched conditions) to reveal the layered structure of the material, before subjecting it to compressive loading at high strain rates. Fig 4 shows optical micrographs at magnifications of up to 600X and Fig 4 shows the SEM (Philips XL 30 SEM) micrograph at a higher magnification. The black spots in Fig 4 are due to inclusions and pits, which are clearly distinguished in the SEM as the inclusions (TiC) appear as bright spots compared to the pits (induced during processing) that appear dark.

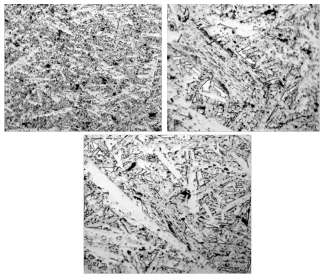

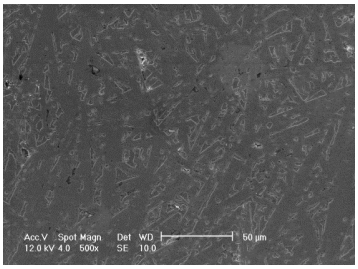

Figure 4. (Left) Optical Micrographs of Ti_2AlCas received (From TAMU) at magnifications a)200X , b)400X and c) 600X, highlighting the layered structure of the material before loading. (Right) SEM Micrograph showing TiC particles as bright spots (blue circles) and pits as dark spots (red circles) distributed throughout the specimen surface.

3.2.2 Microstructural characterization of deformed and fractured specimens

In this sub-section, SEM microstructural characterization of deformed and failed specimens is reported, which reveal the microscopic features associated with deformation. Fig 5 ((a)-(d)) shows the fractured surface of specimens with L-D 0.2 which shows kink band formation with a delaminating layer in the foreground (Fig 5 (a)), grain and nano-laminate *folding* (Fig 5 (b)), with a fibrous appearance, which clearly indicates the ductile nature of this material. Fig 5 (c) shows the mechanism of grain tearing. A portion of a grain is separated into two, in a direction perpendicular to the layered structure. This crack formation is in the vicinity of a kink band, as shown, and possibly initiated at the kink boundary, which are areas of high energy since it contains an array of dislocations. Fig 5 (d) shows a complete folding of nano-laminates and a portion of it lies completely on top of the other portion. Fig 6 ((a)-(d)) shows the microstructural features of the deformed specimen without fracture for specimens tested at L-D 0.4, which show the distribution of rough patches on the surface (Fig 6(a)), with magnified views of patches (Fig 6(b)-(d)). These images clearly show features of deformation similar to kink bands (Fig 6(c)) but these are much less extensive compared to fractured specimens. Fig 6(d) shows relative sliding of layers on top of each other, which is a process initiated by dislocation movement leading to the creation of kink bands.

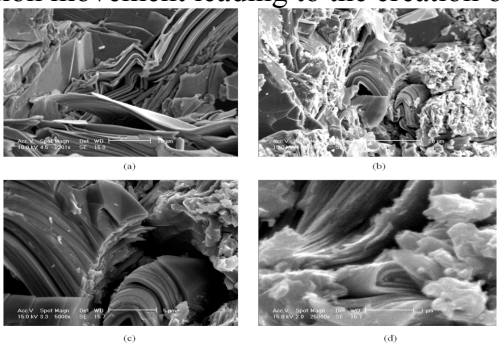

Figure 5. SEM Micrographs of Ti_2AlC after fracture using a specimen of L-D ratio 0.2 at magnifications a) 2,000X showing kink band formations with well defined boundaries, b) 1500X showing grain folding and void formations, c) 5,000X showing cracking through the lamellae at the kink boundary and d) 25,000X showing complete folding of the layers making an angle of almost 0^o.

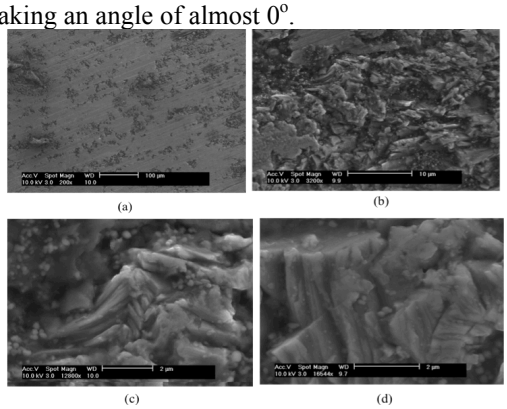

Figure 6. SEM Micrographs of Ti_2AlC after deformation without fracture showing a) distribution of rough patches throughout the surface , b) a zoomed in portion of a pit showing the deformed surface, c) kink band formation and d) sliding of the lamellae.

3.3 Discussion

The high strain rate response of Ti_2AlC was studied at L-D ratios of 0.2, 0.4 and 0.8 (section 2) at strain rates of 500-2500 s^{-1}. The test at L-D ratios of 0.2 and 0.4 on set-up I resulted in elasto-plastic deformation without fracture and the strain signals from the strain gauges were used to obtain strain-time and dynamic stress-strain constitutive behavior, from which material properties were calculated. The strain fields obtained using DIC for specimens with L-D 0.4 showed a certain amount of heterogeneity (~0.5%), which can be explained based on the microstructural observations.

A comparison of the micrographs before deformation (Fig 4) to the micrographs after deformation without fracture (Fig 4) show heterogeneity in the microstructure with rough patch formations of different sizes scattered throughout the specimen surface. The patches observed in the deformed specimen varied in size from 0.1 mm to 1 mm and the heterogeneous strain field regions (Fig 2 and Fig 3) had variation regimes from ~0.2 – 1.4 mm. From this analysis, it was inferred that these rough patches were areas of stress concentrations, which led to relatively higher strains compared to the surrounding areas and hence resulted in a heterogeneous strain field. A closer analysis (at higher magnification of 12000X-Fig 5 (c)) of these rough patches reveal ridge like formations, which are similar in structure to kink bands. A possible mechanism of these patch formation is from the growth and subsequent coalescence of minuscule pits, initially present in the microstructure. The fracture surface (L-D = 0.2) shows kink band formations and delamination resulting from sliding of basal planes (Fig 6(a)), grain and lamellar *folding* which are similar to kink bands but have only one boundary. Two types of folding are shown in Fig 5(b) and (d). At the same time, there were regions where the lamellar stacks formed kink bands, with 2 distinct boundaries and then cracks developed separating the kinked lamellar stack into two halves, as shown in Fig 5 (c). The fibrous appearance of the cracked surface (cross-sectional) suggests that it failed in a ductile manner. Hence, this is termed *grain-tearing*.

$M_{n+1}AX_n$ phase ternary ceramics are nano-laminated materials which exhibit unique combination of properties of both metals and ceramics and hence are attractive for structural applications. In this paper, we reported SHPB testing of Ti_2AlC, a $M_{n+1}AX_n$ phase ternary ceramic at strain rates of 500-2500 s^{-1} using specimens of different L-D ratios (0.2, 0.4 and 0.8) to characterize its behavior under dynamic loading conditions. At L-D ratio of 0.2 and 0.8, the specimens fractured in a brittle manner at a strain rate of 1500 s^{-1} and 2500 s^{-1} respectively. At L-D of 0.2, up to 1200 s^{-1} the material showed a ductile behavior with clearly defined yield points at some strain rates. The dynamic stress-strain constitutive behavior was analyzed for these specimens. The modulus calculated from this analysis had values (35-75GPa) higher than the modulus obtained from quasi-static loading (13 GPa). The mode of deformation during this combined ductile-brittle behavior is due to the formation of kink bands. In order to investigate the nature, size, distribution of kink bands and associated advanced modes of deformation and fracture, microstructural characterization of specimens was done before and after subjecting them to loading. The features revealed advanced deformation modes and a slightly different mechanism of initiation and propagation of fracture processes compared to loading under quasi-static conditions.

References

1. Barsoum MW, El-Raghy T, Radovic M, Ti3SiC2: A Layered Machinable Ductile Carbide, *Interceram. vol 49, Issue 4, pp. 226-233*, 2000

2. Barsoum MW, Radovic M, Elastic and Mechanical properties of the MAX Phases, *Annual. Rev. Mater. Res, pp.9.1-9.33*, 2011

3. Zhou AG et al, Incipient and regular kink bands in fully dense and 10 vol.% porous Ti2AlC, *Acta Materialia, 54, pp.1631-1639*, 2006

4. Zhou AG, Basu S, Barsoum MW, Kinking nonlinear elasticity, damping and microyielding of hexagonal close-packed materials, *Acta Materialia, 56, pp.60-67*, 2008
5. Barsoum MW, El-Raghy T, Room Temperature Ductile Carbides*, Met. and Mat. Trans. A, Vol. 30A , pp.363 - 369*, 1999
6. Barsoum MW et al, Kinking Non-Linear Elastic Solids, *Encyclopedia of Materials: Science and Technology, pp. 1- 22*, 2010
7. Zhou Y.C, Wang X.H, Deformation of polycrystalline Ti2AlC under compression, *Mat Res Innovat, 5, pp.87 - 93*, 2001
8. Poon et al, Damage accumulation and hysteretic behavior of MAX phase materials, *Journal of the Mechanics and Physics of Solids, Vol. 59, Issue 10, pp.2238 -2257*, 2011
9. Kolsky H, An investigation of the mechanical properties of materials at very high rates of loading, *Proceedings of the Physical Society B, Vol. 62, pp.676 -700*, 1949
10. Gama et al, Hopkinson bar experimental technique: A critical review, *Applied Mechanics Review, Vol. 57, Issue 4, pp.223 -250*, 2004
11. Subhash G, Ravichandran G, Split-Hopkinson pressure bar testing of ceramics, *ASM Handbook, Vol. 8, Mechanical Testing and Evaluation, pp.488-496*, 2000
12. Al-Mousawi M M, Reid S R and Deand W F, *Proceedings of Institution of Mechanical Engineers*, *Vol. 211, Part C, pp.273-292*, 1997
13. Yuan J, Takeda N, Waas A, A note on data processing in the split pressure bar tests, *Experimental Techniques*, pp. 21-24, 1998
14. Lifshitz J M, Leber H, Data Processing in the Split Hopkinson Pressure Bar Tests, *International Journal of Impact Engineering*, *vol 15, Issue 6, pp. 723-733*, 1998
15. Pankow M, Attard C, Waas A M, Specimen size and shape effect in split Hopkinson pressure bar testing, *The Journal of Strain Analysis for Engineering Design,vol 4, pp.689-698,* 2004